S. Ahmad, Y. Liu, S.A. Khan, M. Hao, X. Huang (2023) *Hybrid battery thermal management by coupling fin intensified phase change material with air cooling*, **Journal of Energy Storage**, 64, 107167. https://doi.org/10.1016/j.est.2023.107167

Hybrid battery thermal management by coupling fin intensified phase change material with air cooling

Shakeel Ahmad[a], Yanhui Liu[a,b], Shahid Ali Khan[c], Menglong Hao[d], Xinyan Huang[a,c,*]

[a] *Department of Building Environment and Energy Engineering, The Hong Kong Polytechnic University, Hong Kong*

[b] *The Hong Kong Polytechnic University Shenzhen Research Institute, Shenzhen, China*

[c] *Department of Mechanical Engineering, City University of Hong Kong, Hong Kong*

[d] *School of Energy and Environment, Southeast University, Nanjing, China*

***** Corresponding to *xy.huang@polyu.edu.hk*

Abstract

Phase change material (PCM) based passive battery thermal management (BTMS) is a promising strategy for controlling lithium-ion battery temperature during operation. However, the drawbacks of low thermal conductivity and poor secondary heat dissipation of PCM still need to be addressed. Herein, the metal fin intensified PCM system coupling with air cooling is proposed for battery thermal management. The effects of PCM thickness, metal fin diameter and number, air inlet velocity, and airflow temperature on the performance of the proposed BTMS are numerically investigated. Results indicate that the novel hybrid BTMS exhibits a superior cooling performance than fin-air BTMS without PCM and PCM-air BTMS without fins, reducing the maximum battery temperature by 18.6% and 3.2%, respectively. The embedded fins can improve the heat dissipation of the battery and PCM. Increasing air velocity can help recover the PCM latent heat but consume additional power. The proposed BTMS is investigated and optimized considering the cooling performance and power consumption tradeoff. The optimal design has a 1.0 mm PCM thickness, 162 fin numbers, and a 3.0 mm fin diameter. Under such an optimal design, battery temperature can be controlled below the desired value of 40℃ with less power consumption. The run-out of PCM latent heat is also effectively prevented in continuous cycle operation with an air velocity of 2.0 m/s. This study can provide a new insight into an advanced BTMS design for next-generation battery systems with high charging and discharging rates.

Keywords: *Thermal management system; air cooling; fin diameter; fin number; phase change material.*

Nomenclature

A	area (m^2)	**Greeks**	
C_p	heat capacity ($J/kg \cdot K$)	β	PCM liquid fraction
d_p	diameter of metal fin (m)	μ	dynamic viscosity (Pa s)
D_h	hydraulic diameter (m)	ρ	density (kg/m^3)
q_{gen}	heat generation rate (W)	Δ	difference
h_p	height of metal fin (m)		
H	enthalpy (J)	**Subscripts**	
k	thermal conductivity ($W/m \cdot K$)	amb	ambient
L	latent heat (J/kg)	b	battery
p	static pressure (Pa)	c	coolant
P_{ac}	ideal refrigerating power (W)	in	inlet
P_c	total power consumption (W)	S	solid
P_{fan}	fan power (W)	L	liquid
Re	Reynolds number		
s_h	pitch distance along horizontal direction (m)	**Abbreviations**	
s_v	pitch distance along vertical direction (m)	BTMS	battery thermal management system
t	Time (s)	COP	coefficient of performance
T	temperature (℃)	Li-ion	lithium-ion
u_{in}	inlet air velocity	$LiFePO_4$	lithium iron phosphate
v	velocity (m/s)	PCM	phase change material
ν	kinematic viscosity (m^2/s)	SIMPLE	semi-Implicit Method for Pressure Linked Equations
w_{PCM}	PCM thickness (m)	UDF	user defined function
w_T	thickness of spacing around the battery (m)		

1. Introduction

The energy crisis, air pollution and climate change are critical issues faced by people worldwide and urgently need to be addressed. Greenhouse gas emission is one of the main reasons for climate change issues. According to the International Energy Agency 2016, the transport sector was the second majorly contributing sector to greenhouse gas emissions. The development of electric vehicles and energy storage systems for microgrids is a solution to minimize our dependence on fossil fuels and mitigate air pollution and global climate change impacts, leading to improved urban air quality. The lithium-ion (Li-ion) batteries are widely used as energy storage systems in electric vehicles [1] and electric grids due to their advantages, including high energy density, power density, long cycle life and low self-discharge compared to the other kinds of rechargeable batteries [2]. However, the performance of Li-ion batteries strongly depends on their operating temperature. To maximize the battery lifespan and enhance its power capacity, the operating temperature should be kept in the optimal range of 25-40 ℃ [3]. During the high discharge rate, a huge amount of heat is produced owing to exothermic chemical reactions [4]. If the heat cannot be removed in time, the side reactions inside the batteries will be triggered, which will cause capacity degradation or even thermal runaway [3]. Therefore, an excellent-performing BTMS is essential to ensure the battery works at optimal temperature. In addition to homogenizing cell temperature, BTMS should be lightweight, reliable and draw low parasitic power.

Considering the cooling medium, the BTMSs can be classified into air cooling [5-7], liquid cooling [8, 9], and phase change material (PCM) cooling [10]. In air cooling, the operating temperature is controlled by flowing air over the battery pack [6], and it has been commercially used in vehicles such as Honda Insight and Toyota Prius [11]. Although air cooling is famous for its simple structure, lightweight, electrical safety and low cost [2, 12], the relatively low cooling efficiency hinders its further application. Liquid cooling is more effective, but it suffers from the issues like more weight, coolant leakage, design complexities and higher cost [2, 13]. Air and liquid are active cooling methods that restrict battery temperature at the cost of external energy consumption.

On the other hand, PCM-based BTMS is a passive cooling method and gained increasing research attention in recent years. Although the PCM can store thermal energy in both sensible and latent forms, the advantage of latent heat is mainly utilized by PCM-based BTMS to absorb battery heat generation and reduces battery temperature without consuming external energy [2, 13, 14]. To further enhance the cooling performance, the combination of both active and passive BTMSs is an emerging topic and attracts considerable research efforts. Many different types of hybrid BTMSs, including PCM/liquid [10, 15] and PCM/heat pipe/liquid BTMS [16], have been proposed, which provide potentially effective cooling to the battery pack.

Particularly, BTMS, with the combination of air cooling and PCM, offers the potential advantages of simple design, low cost, lightweight and reliability for thermal management applications.

PCM cooling was first shown by Al-Hallaj and Selman [17], and PCMs are a promising candidate for latent energy storage [18, 19]. Nevertheless, during prolonged operations with multiple charge/discharge cycles, the PCM latent heat may completely run out, leading to the failure of BTMS. In addition, extremely high heat generation at higher charge/discharge rates may exceed the thermal management capacity of the PCM. The hybrid BTMS that couples passive PCM cooling with active cooling, such as air cooling, can effectively address such issues [20, 21]. Bamdezh and Molaeimanesh [20] combined air cooling with PCM encompassing the cylindrical cells and studied the effects of cell arrangement and thickness of the PCM layer. The proposed hybrid BTMS was able to maintain the remarkable capability of uniform temperature distribution never exceeding 1.5 ℃ for all cases. Ling et al. [21] proposed a hybrid BTMS which integrates PCM with air cooling for cylindrical cells. It successfully mitigated the heat accumulation and restricted the maximum temperature to under 50 ℃. Fathabadi [22] combined the air cooling through thin ducts with PCM cooling for the prismatic battery pack and demonstrated that the proposed hybrid BTMS could maintain the temperature distribution of the pack under 60 ℃.

Mehrabi-Kermani [23] integrated PCM with air convection over pin fin heat sink and observed that the hybrid BTMS kept the temperature below 60 ℃ at an air speed of 3.2 km/h. However, the pin fins were not embedded inside the PCM, and heat generation was carried out using a simplified film heater instead of the cuboid shape of the prismatic battery. The roles of pin fins on thermal conductivity and air flowing over practical cuboid shape of a prismatic battery had not been elucidated. Jilte et al. [24] proposed the cell-to-cell arrangement for the hybrid BTMS for a cylindrical battery pack with PCM and air, and demonstrated that PCM around each cell improved heat dissipation and temperature uniformity. Lv et al. [25] coupled a stable shape serpentine composite PCM structure with air cooling in the channels for the cylindrical battery pack, which reduced the temperature to a much smaller value (51.9 ℃) than block-shaped composite PCM at the same fan power. Jiang et al. [26] found that baffles improve fluid interactions and upgrade the heat transfer efficiency in air and PCM hybrid BTMS for tube-shell packs with cylindrical batteries. Qin et al. [27] showed that air and PCM hybrid BTMS could effectively control the maximum temperature and temperature difference in the recommended range.

Then, in general, pure PCMs have an undesirably low thermal conductivity [28], and make it difficult to achieve faster heat transfer during melting and solidification processes posing critical challenges at higher charge/discharge rates. In order to enhance the PCM thermal conductivity, different strategies such as additives, metal foam [29] and carbon fiber have been used. However, additives face risks of agglomeration problems and settle down at the bottom [30]. Another popular method to improve thermal conductivity is

the insertion of metal fins [31, 32]. Metal fins have been proven to be effective in increasing heat transfer in PCM structures. Due to the advantages of structure simplicity, easy manufacturing and low cost, they have been extensively used for heat transfer augmentation in PCMs [33-35]. Ali and Arshad [31] used circular fins for the thermal conductivity enhancement of PCM for electronic cooling. Liu et al. [36] used honeycomb fins for BTMS performance improvement. The effects of the thickness of PCM and fins and the gap between fins for PCM-based BTMS were investigated by Ping et al. [37]. Weng et al. [38] studied the effects of multi-channel fins and found that these fins could increase the secondary cooling capacity of PCM.

It is observed from the above discussion that the PCMs can provide excellent passive thermal management, but in prolonged operations and with multiple charge/discharge cycles, their latent heat may completely run out resulting in the failure of BTMSs. When PCM cooling is combined with air cooling, the resulting hybrid BTMS can maintain battery temperature, but previous studies were mostly focused on cylindrical batteries, and the comprehensive studies for hybrid air/PCM BTMS for prismatic batteries are sporadic. The pure PCM has low thermal conductivity, which can be improved by inserting fins in the PCM, effectively increasing heat transfer with the accompanying advantages of structure simplicity, easy manufacturing and low cost. Metal fins improve the heat transfer capability of PCM-based passive BTMS, but the understanding of air cooling over pins for the cuboid shape of a prismatic battery has not been explored.

In this work, a novel hybrid BTMS with PCM-embedded fins combined with forced air convection over fins has been investigated. The performance of the novel hybrid BTMS is compared to the BTMS without PCM and fins completely exposed to air cooling and BTMS with PCM and air cooling but no fins. The effects of PCM thickness, fin diameter and fin number, inlet velocity and temperature on the performance of the novel hybrid BTMS are investigated. Then, cyclic tests are conducted to assess the prolonged performance of the novel hybrid BTMS.

2. Physical Problem Description

In the present work, a prismatic $LiFePO_4$ battery with a metal casing has been adopted from the experimental work [39]. The battery core dimensions and physical properties are selected as given in the work [39]. The battery core is enclosed by the metal casing and has the size of 15.6 mm (x) × 77.6 mm (y) × 103 mm (z) and that of metal casing 17 mm (x) × 79 mm (y) × 104.7 mm (z). The rated capacity and nominal voltage of the battery are 8.0 Ah and 3.2 V, respectively. The anode and cathode are made of graphite and lithium iron phosphate, respectively, and aluminum-foil and copper-foil are used for positive and negative current collectors. For simplicity, battery tabs are not modelled.

As illustrated in Fig. 1b, the prismatic cell is surrounded by the PCM layer with embedded metal fins. In Fig. 1c, a single battery with a symmetric boundary on the sides is considered, where the symmetric boundary is reasonable, as a battery in a pack can have multiple neighboring batteries on its sides [5]. A spacing of 10 mm between two neighboring batteries [37] in a battery pack and a thickness of 3 mm for PCM layer wrapped on small peripheral sides [40] of the battery have demonstrated good thermal performance. In the present work, taking into account the symmetrical nature of the problem, half of the total spacing around the battery, that is $w_T = 5.0\ mm$, is chosen, which is used for battery cooling through the PCM layer and air flow (Fig. 1b). Out of total $w_T = 5.0\ mm$ spacing, a thickness $w_{PCM} = 0.25 - 3.0\ mm$ is used for the PCM layer, and the remaining spacing is used for air flow. The air enters from the inlet at the bottom and exits from the outlet at the top.

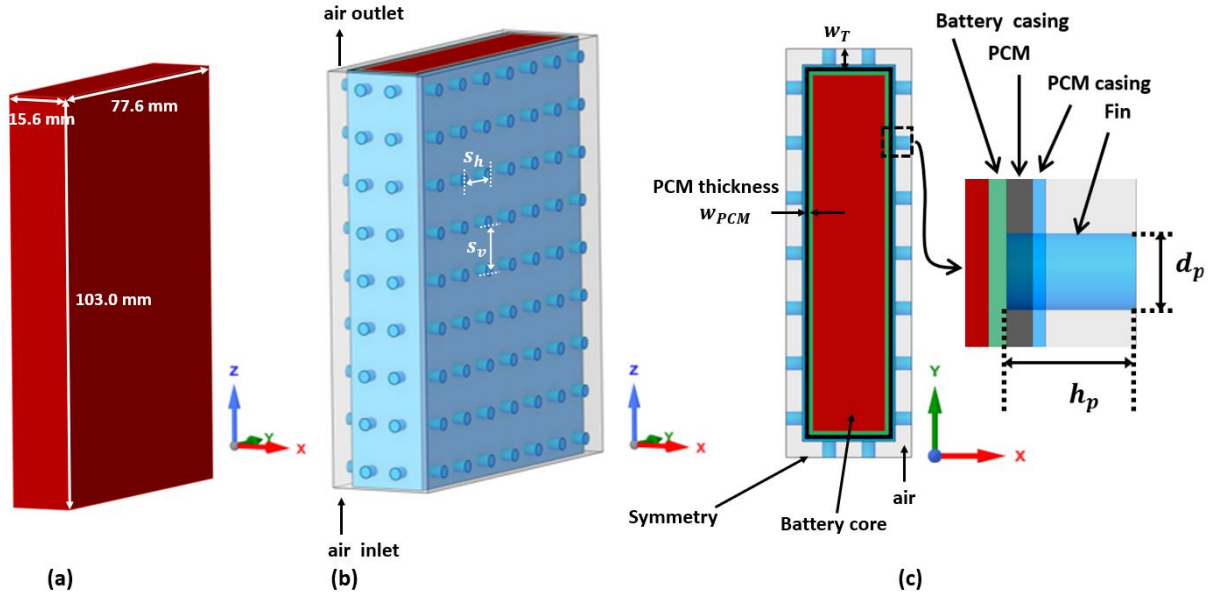

Fig. 1. Schematic diagrams of (a) battery core, (b) the PCM-Fin-Air BTMS and (c) zoomed-in-view of the PCM layer around the battery and embedded metal fin.

During the PCM melting process, the phase change from solid to liquid takes place, and a metal casing around the PCM is usually used to avoid leakage [41]. The PCM metal casing of thickness 0.5 mm is shown in Fig. 1b. The cylindrical fins are attached to battery casing and protrude through the PCM and air such that a part of fin is inside PCM, whereas the other part is exposed to forced air cooling (Fig. 1b). The PCM casing and fins are generally made from copper or aluminium, but aluminium is favored due to its lower cost and lightweight. The diameter of the fins is $d_p = 3.0\ mm$, and the height staring from battery casing is fixed to be $h_p = 5.0\ mm$. During the battery discharge process, heat is generated in the battery and transferred as sensible heat to PCM.

When the temperature exceeds the melting temperature of PCM, a part of the energy will be transformed into latent heat, triggering the PCM phase change to liquid. The air flowing through the bottom inlet over the fins and metal casing of PCM helps absorb a large amount of heat and recover the latent heat, and thus, can potentially prevent the complete melt out of PCM. The air can be provided by a fan or cooled air below ambient temperature using a fan accompanied by a heat exchanger. The key parameters of the proposed BTMS are summarized in Table. 1.

Table 1. Thermophysical properties of Li-ion battery [39] and PCM [42].

Properties		Battery core	Battery metal casing	PCM casing and fins	PCM-RT35HC [42]
Density (solid)	$\rho_s(kg/m^3)$	2181	2800	2719	880
Density (liquid)	$\rho_l(kg/m^3)$				770
Latent heat	$L\ (k\,J/kg)$				240
Thermal conductivity	$k\ (W\ /m\ K)$	$k_x = 0.54,$ $k_y = k_z = 21.9$	170	202.4	0.2
Heat capacity	$C_p(J\ kg^{-1}K^{-1})$	3.2 T +1177	880	871	2000
Solidus temperature	T_s(℃)				34
Liquidus temperature	T_L(℃)				36

3. Governing Equations

The energy conservation equation [39] for the Li-ion battery is written as

$$\rho_b C_{p,b} \frac{\partial T_b}{\partial t} = \nabla \cdot (k_b \nabla T_b) + \dot{q}_{gen} \quad (1)$$

where ρ_b, $C_{p,b}$, k_b , and T_b are density, specific heat capacity, thermal conductivity and temperature of battery. $\dot{q}_{gen}$ is the volumetric heat generation rate of the battery, which represents the sum of joule heat, irreversible heat and reversible heat. Sheng et al. [39] experimentally measured the heat generation rate during the discharge process for $LiFePO_4$ battery at high current rates (C) of 9 C, 7 C and 5 C under an ambient temperature of 30 ℃. The C-rate is referred as the measurement of the charge or discharge rate of battery relative to its nominal capacity. The heat generation rate q_{gen} (W) for symmetrical half of battery core is written as [39]

$$q_{gen} = a_o + a_1 t + a_2 t^2 + a_3 t^3 \quad (2)$$

In this work, the battery heat generation rate for the discharge cycle at a high C-rate of 5 C, which is a representative higher C-rate [12], is used. The coefficients of the polynomial are given as follows [39];

$a_o = 4.28$, $a_1 = 4.19 \times 10^{-2}$, $a_2 = -1.62 \times 10^{-4}$ and $a_3 = 2.07 \times 10^{-7}$. Volumetric heat source is obtained from heat generation rate q_{gen} divided by volume. A user-defined function (UDF) code is developed to realize the volumetric heat source.

The governing equations for the heat transfer in PCM are given as follows

$$\rho_{PCM} \frac{\partial H_{PCM}}{\partial t} = \nabla \cdot (k_{PCM} \nabla T_{PCM}) \tag{3}$$

$$H_{PCM} = \int_{T_0}^{T} C_{PCM} dT + \beta L \tag{4}$$

where ρ_{PCM}, H_{PCM}, k_{PCM} represent the density, enthalpy and thermal conductivity of the PCM. T_0 and T are PCM temperature and ambient temperature, L is the latent heat, and β is the PCM liquid fraction. The PCM liquid fraction depends on the temperature and is given as

$$\beta = \begin{cases} 0 & T < T_s \\ \frac{T - T_s}{T_l - T_s} & T_s \leq T < T_l \\ 1 & T \geq T_l \end{cases} \tag{5}$$

where the PCM liquid fraction change from 0 (solid) to 1 (liquid).

For the airflow, the governing equations for the continuity, momentum and energy relations [43] are:

$$\frac{\partial \rho_c}{\partial t} = \nabla \cdot (\rho_c \vec{v}_c) = 0 \tag{6}$$

$$\rho_c \frac{\partial \vec{v}_c}{\partial t} = \rho_c (\vec{v}_c \cdot \nabla) \vec{v}_c = -\nabla \mathrm{p} + \nabla \cdot (\mu_c \nabla \vec{v}_c) \tag{7}$$

$$\rho_b C_{p,c} \frac{\partial T_c}{\partial t} + \nabla \cdot \left(\rho_c C_{p,c} \vec{v}_c T_c\right) = \nabla \cdot (k_c \nabla T_c) \tag{8}$$

where ρ_c, $\vec{v}_c$, $C_{p,c}$, k_c, T_c, p and μ_c are density, velocity vector, specific heat capacity, thermal conductivity, temperature, static pressure and dynamics viscosity, respectively, for the cooling air.

For the fins and metal casings, the energy conservation equation can be expressed as follows:

$$\rho_h C_{p,h} \frac{\partial T_h}{\partial t} = \nabla \cdot (k_h \nabla T_h) \tag{9}$$

where ρ_h, $C_{p,h}$, K_h and T_h are density, specific heat capacity, thermal conductivity and temperature, respectively, for the fins and metal casings.

The boundary condition:

$$T(x, y, z) = T_{amb}, \quad t = 0 \tag{10}$$

where T_{amb} represents ambient temperature.

The boundary condition at the interface between battery core and metal casing

$$-k_b \frac{\partial T}{\partial n} = -k_{h,b} \frac{\partial T}{\partial n} \tag{11}$$

The boundary condition at the interface between battery metal casing and PCM

$$-k_{h,b} \frac{\partial T}{\partial n} = -k_{PCM} \frac{\partial T}{\partial n} \tag{12}$$

The boundary condition at the interface between PCM and aluminium casing around PCM and fins

$$-k_{PCM} \frac{\partial T}{\partial n} = -k_{h,pcm,f} \frac{\partial T}{\partial n} \tag{13}$$

The boundary condition at the interface between PCM casing and fins and that of cooling air

$$-k_{h,pcm,f} \frac{\partial T}{\partial n} = -k_c \frac{\partial T}{\partial n} + h_c(T_c - T_{h,pcm,f}) \tag{14}$$

where $T_{h,pcm,f}$ is surface temperature of PCM casing and fins.

The boundary condition at the top and bottom faces is natural convection with a heat transfer coefficient of $h = 3.25\, W/m^2K$ [39]. The interfaces between the battery, PCM and fins are thermally coupled. The no-slip velocity condition is considered at walls. Velocity inlet boundary condition at the bottom inlet (Fig. 1) and pressure outlet at the top outlet are applied.

To simplify the simulation model, some assumptions are made as follows

- The thermal and physical properties of the metal materials are considered to be independent of temperature since the range of temperature change is narrow in this work.
- Variation of PCM volume during the phase change process is ignored. Liquid motion in PCM is not considered.
- Heat generation inside the battery is uniform.
- Radiation heat transfer is ignored.
- The contact resistances between the battery, PCM, and fins are ignored.

The governing equations are solved using the commercial CFD package, ANSYS FLUENT. The second-order upwind scheme is used for discretizing momentum and energy equations, whereas pressure correction is achieved via the PRESTO scheme. For pressure-velocity coupling Semi-Implicit Method for Pressure Linked Equations (SIMPLE) algorithm is used. To achieve the convergence condition, the residual criteria of 10^{-4} and 10^{-6} is employed for the flow and energy equations, respectively. The Reynolds number is calculated as $Re_D = u_{in} D_h/\nu$. D_h is hydraulic diameter [44], and the air kinematic viscosity is considered

to be $1.6 \times 10^{-5}\ m^2/s$. For inlet air velocity the of $1.0\ m/s$, the Reynolds number is 436. The flow is laminar; hence, the laminar model is used.

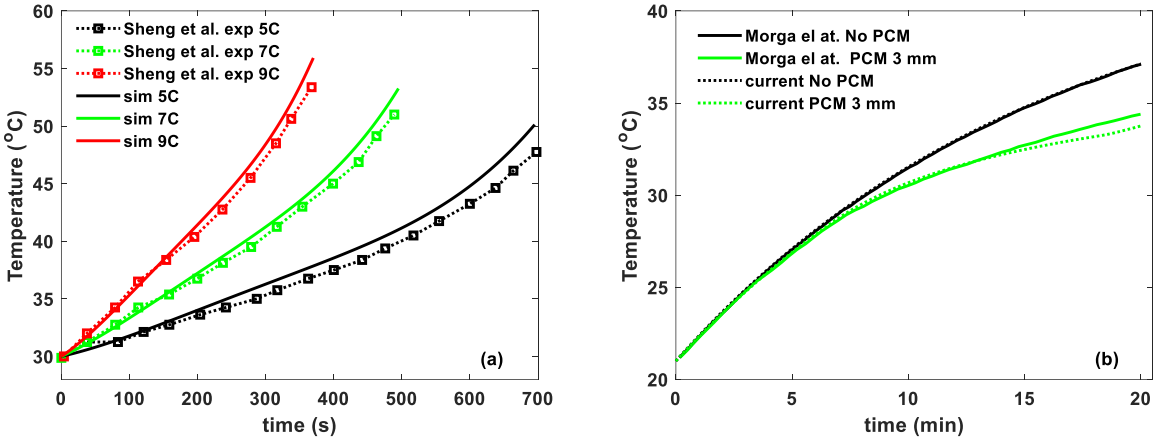

Fig. 2. Comparison of current results with (a) published experimental results without PCM at different C-rates and (b) with published results of PCM based BTMS.

The CFD model is first validated for a single prismatic battery. The physical model of the battery and boundary conditions are similar to those described in the experiment [39]. The comparisons of the battery temperature between simulation and experiment measurements at high C-rates of 5 C, 7 C and 9 C during the discharge process are shown in Fig. 2a. Overall, simulation results are in good agreement with the experiment, and the error is less than 5%, which shows the good accuracy of the model. Then, the CFD model was verified for PCM-based BTMS with PCM located on small peripheral sides of the battery against the results obtained by Moraga et al. [45]. The thickness of the PCM layer is $3\ mm$ [45], and the comparisons of battery temperature with/without PCM cases against Moraga et al. [45] are shown in Fig. 2b. The error is found to be less than 5%, again confirming the accuracy of the model.

The mesh of BTMS is generated using Tetrahedral meshing in ANSYS. The mesh quality has a big influence on the accuracy of numerical results. In this work, the quality of the mesh is checked in terms of the grid independence test. In addition, time step independence test has been carried out. Simulations for five different gird numbers, including 157964, 243617, 1310754, 2364643 and 4954447 and five time-steps, i.e., 0.25, 0.5, 1.0, 1.5 and 2.0 s are conducted. The battery temperature is shown in Fig. 3. The grid number 1310754 and time step 1.0 s have maximum errors of 0.48% and 0.2% when compared to the largest grid size and smallest time step, respectively. It shows that increasing the grid number does not change results considerably. Therefore, the grid number 1310754 and time step 0.5 s are selected for simulations.

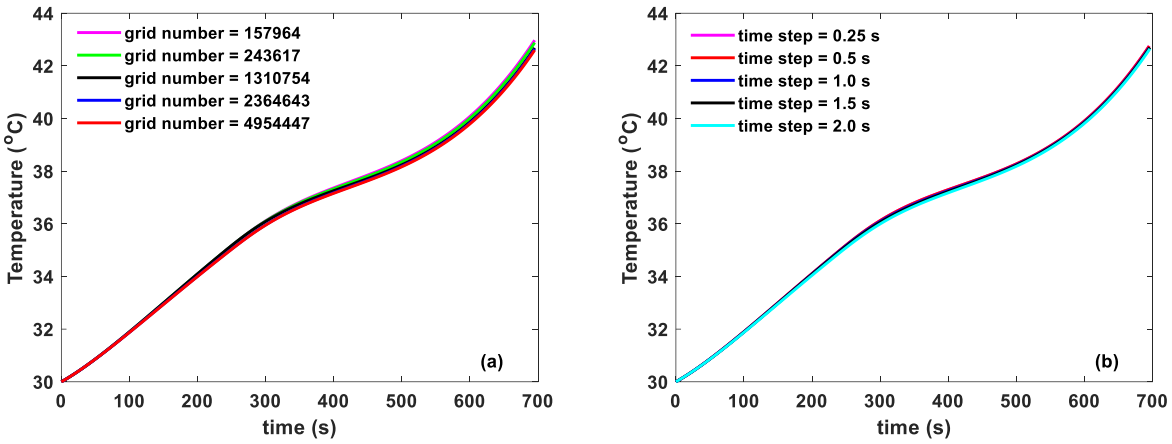

Fig. 3. Independence tests of battery temperature for (a) grid number and (b) time step.

4. Results and discussion

The performance of the novel hybrid PCM-Fin-Air BTMS is exhibited by the thermal response of the battery and the melting behavior of PCM in the discharge process. A widely used and commercially available PCM -RT35HC [10, 42] (Table. 1) with a thickness of $w_{PCM} = 1\ mm$ is wrapped around the sides of the battery. Fins are embedded in the PCM with a uniform pitch distance of $s_h = 12\ mm$ and $s_v = 12\ mm$ along the horizontal and vertical directions, respectively. But, due to the small peripheral width of battery, i.e., $17\ mm$, the horizontal pitch distance s_h for the peripheral sides is fixed at $8.5\ mm$ for all simulation cases. The total number of fins is found to be 162, and the height and diameter of the fin is $d_p = 3\ mm$ and $h_p = 5\ mm$, respectively. The cooling air enters from bottom with inlet velocity of $1.0\ m/s$ and exits from top. The inlet air temperature and initial battery temperature are set equivalent to the ambient temperature 30 ℃.

The variation of battery temperature with time is shown in Fig. 4. The heat generated in the battery during the discharge process is transferred to fins and PCM. The PCM has low thermal conductivity, but it is augmented by the embedded fins [30], effectively decreasing the overall thermal resistance. The higher thermal conductivity of fins provides alternative pathways for heat flow. These new pathways help in quickly dissipating heat by two methods: the heat transfer to deep layers of the PCM [35] and air convection over the fin parts located in the air region.

During the battery discharge process, sensible heat transfer first occurs, increasing the PCM temperature. However, the heat generated in the battery is lower than the heat required to melt the PCM, and the liquid fraction value remains zero until the time $t < 200\ s$ (Fig. 4). In this period, heat transfer occurs in the sensible form to PCM and thorough PCM casing and fins to airflow. In the later stage $t > 200\ s$, the heat

is added to PCM in the sensible form and latent heat form, melting the PCM as seen by increasing liquid fraction in Fig. 4.

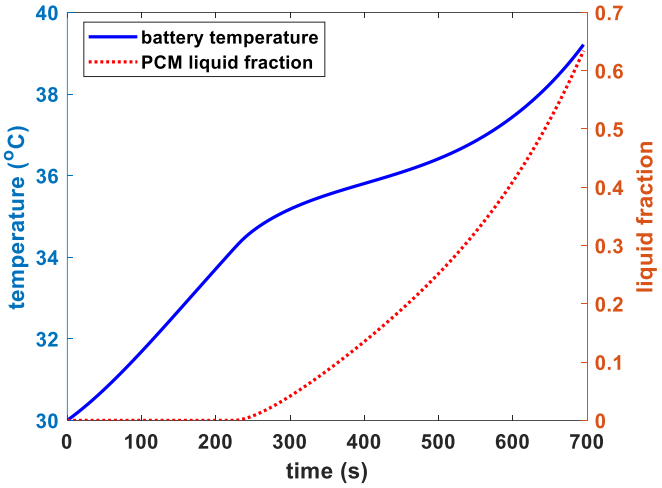

Fig. 4. Evolution of battery temperature and PCM liquid fraction for the novel hybrid PCM-Fin-Air BTMS.

The PCM absorbs more heat, reducing the rate of temperature increase. From time $t = 200\ s$ to the end of battery discharge at $t = 695\ s$, a part of the heat is continually added to PCM, and the other part is dissipated to the air convection over the fins, which combinedly manages to restrict the maximum temperature of battery at the end of the cycle to 39.2 ℃. It is clearly observed that at the end of the discharging cycle, the liquid fraction is less than 1.0 (see Fig. 4), meaning that PCM is not completely melted. It can be concluded that even a smaller thickness of PCM (1 mm), when combined with fins and forced air cooling, can maintain the battery temperature below the desired value of 40 ℃.

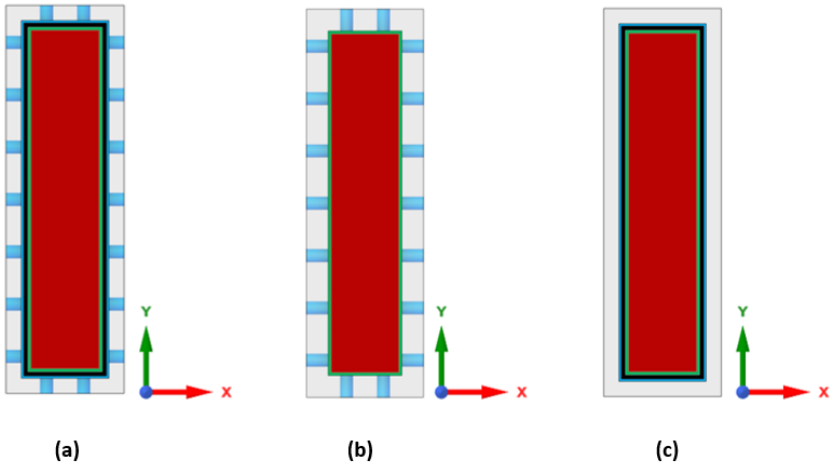

Fig. 5. Top view of different BTMSs (a) novel hybrid BTMS with PCM, air cooling and embedded fins (PCM-Fin-Air BTMS), (b) BTMS with fins and air cooling (Fin-Air BTMS), and (c) BTMS with PCM and air cooling (PCM-Air BTMS).

To further understand the performance of the novel hybrid PCM-Fin-Air BTMS (Fig. 5a), comparisons are made with two different BTMSs: the Fin-Air BTMS and PCM-Air BTMS. The Fin-Air BTMS have fins attached to the battery (see Fig. 5b) but does not have PCM wrapped on the battery sides, and the whole length of $5.0\ mm$ of fins is used for air convection. PCM-Air BTMS lacks fins (see Fig. 5c), while air convection happens only on the PCM metal casing. The comparisons of the battery temperature for different BTMS are shown in Fig. 6a. The temperature trends are nearly similar in the beginning ($t = 200\ s$), but at a later time temperature becomes highest for the Fin-Air BTMS, which is due to the reason that air has low thermal conductivity and is unable to remove enough heat from the battery.

As for PCM-Air BTMS, the battery temperature is quickly dropped due to heat absorbed by PCM and air convection over the PCM metal casing. When the fins are added to BTSM, it reduces the thermal resistance of the PCM and also increases the heat transfer area in the airflow region, resulting in a further decrease in the battery temperature for the PCM-Fin-Air BTMS. The maximum temperature at the end of the discharge cycle for three different BTMSs is shown in Fig. 6b. The battery temperature is highest for the Fin-Air BTMS of 48.2 ℃, which is beyond the best working temperature [3, 46]. When PCM is combined with air cooling without fins, the battery temperature is reduced by 15.4% to 40.7 ℃ in comparison to Fin-Air BTMS. On the other hand, the novel PCM-Fin-Air BTMS reduced the temperature by 18.6% to 39.2 ℃ as compared to Fin-air case. Hence, it can be concluded that the novel PCM-Fin-Air BTMS, due to the embedding of fins in PCM and coupling with air convection, showed the best performance and effectively restricted the battery temperature.

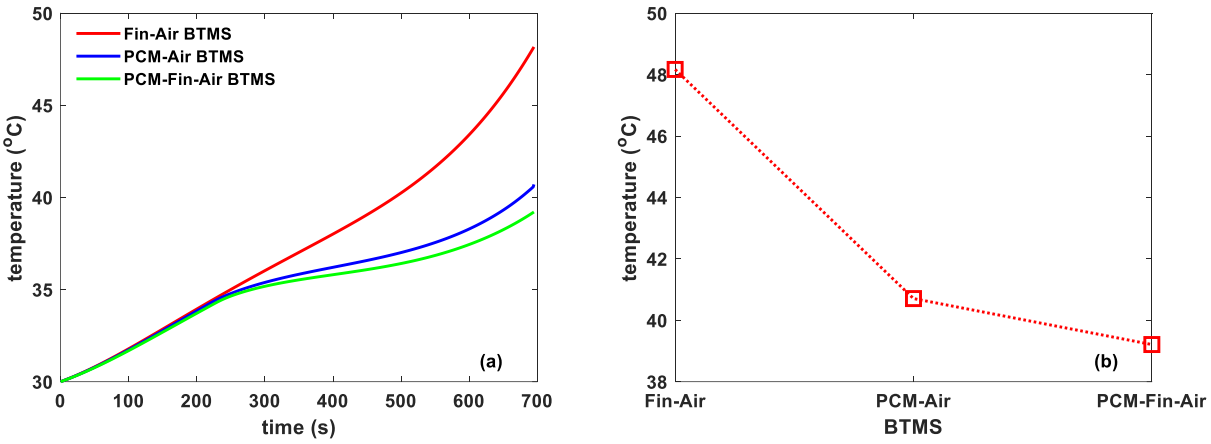

Fig. 6. Comparisons of (a) evolution of battery temperature and (b) maximum battery temperature at the end of discharge cycle for different BTMSs.

4.1 Effects of PCM thickness

To study the effects of PCM thickness on the performance of novel PCM-Fin-Air BTMS, different thicknesses, i.e., $w_{PCM} = 0\,mm$, $0.25\,mm$, $0.5\,mm$, $1.0\,mm$, $2.0\,mm$ and $3.0\,mm$ under the same ambient temperature 30 ℃ and air inlet velocity $1.0\,m/s$ are considered. The thickness $w_{PCM} = 0\,mm$ case represents BTMS having no PCM layer. The influence of PCM thickness on the battery temperature is shown in Fig. 7a. Initially, the trends are similar until time $t = 200\,s$. In the later part ($t > 200\,s$) of the discharge cycle, the temperature increases quickly for smaller values of thickness. For the PCM thickness $w_{PCM} = 0.25\,mm$, the PCM liquid fraction quickly jumps to unity (see Fig. 7c) at time 550s, which means that PCM is completely melted and heat accumulation at a rapid pace takes place in the subsequent stage of the discharge cycle, resulting in the sharp increase in temperature to 44.2 ℃.

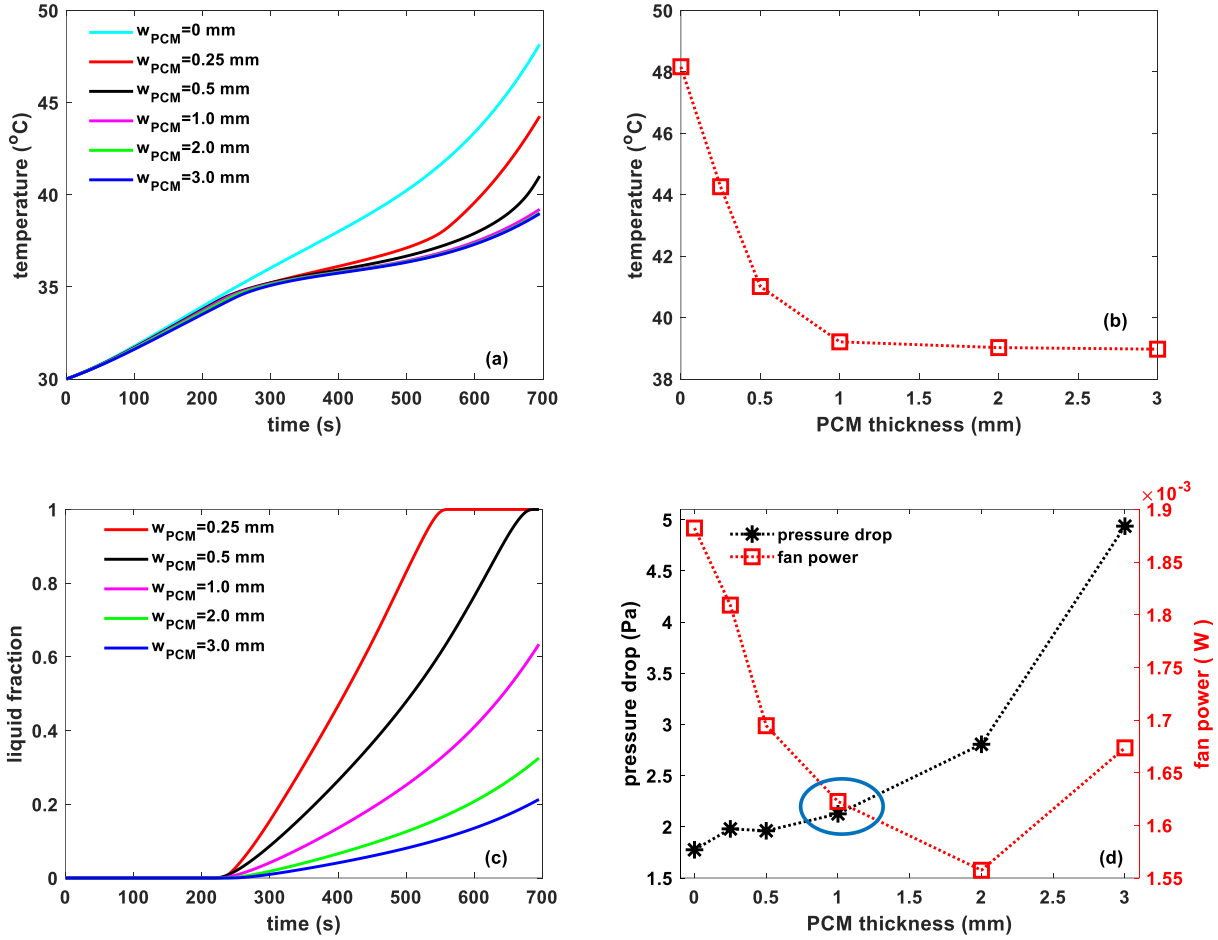

Fig. 7. Comparisons of (a) evolutions of battery temperature and (b) maximum battery temperature at the end of the discharge cycle, (c) evolutions of PCM liquid fraction and (d) fan power and pressure drop for different thicknesses of PCM. The ellipse represents the optimum value of PCM thickness.

The complete melting of PCM is also observed for thickness $w_{PCM} = 0.5\ mm$, but the battery temperature is dropped to a relatively lower value of 41.0 ℃. However, when the thickness is increased to $w_{PCM} = 1.0\ mm$, the PCM liquid fraction at the end of the discharge cycle is found to be 0.63, implying that only a portion of PCM is melted and battery temperature falls to 39.2 ℃ that is within the optimum range. The thick PCM has a lower battery temperature in consistency with work [37]. However, with a further increase in PCM thickness, the PCM liquid fraction is further decreased at the end of the discharge cycle, but there is no appreciable decrease in the temperature, as shown in Fig. 7b.

In addition to battery temperature and PCM liquid fraction, the energy consumption due to the fan is another important criterion for BTMS performance. It is noted that when the thickness of PCM is increased, the inlet area for airflow and heat transfer area of fins in contact with air are decreased. With varying the inlet area at the same air velocity, the fan power consumption changes. The ideal energy consumption due to fan airflow is calculated using the following equation [44, 47]

$$P_{fan} = \Delta P \cdot V = \Delta P \cdot u_{in} A_{in} \tag{15}$$

where ΔP is the pressure drop, which is calculated by the subtraction of outlet pressure from inlet pressure. u_{in} is the inlet velocity. A_{in} is the total area of inlet. In this work, inlet and outlet pressure values averaged over simulation time are used to calculate the pressure drop.

It can be seen in Fig. 7d that the pressure drop is smaller when the PCM thickness is smaller and increases slightly up to the thickness $w_{PCM} = 1.0\ mm$, and subsequently, dramatically increases due to the very thin air inlet area. The Fan power is higher with a smaller PCM thickness, as the inlet area is larger, which allows more air to pass through the inlet. Then, it decreases until $w_{PCM} = 2.0\ mm$ and later increases at $w_{PCM} = 3.0\ mm$ due to a sharp increase in pressure drop (Fig. 7d). It can be seen that the battery temperature is under 40 ℃ when PCM thickness is $w_{PCM} \geq 1.0\ mm$. Though, fan power is slightly smaller at $w_{PCM} = 2.0\ mm$ but increasing thickness adds extra weight to BTMS, making it heavier and more complex in structure as well as costly for practical applications. Hence, the PCM thickness $w_{PCM} = 1.0\ mm$ with moderate fan power and pressure drop (see ellipse in Fig. 7d) found to be optimum and can maintain the battery temperature under the desired value.

4.2. Effects of the fin number

In this section, the fin pitch distance is changed to understand the effects of fin number on the novel hybrid BTMS's ability to restrict the battery temperature rise. The pitch distance is uniformly changed along the horizontal and vertical directions. The different pitch distances, i.e., 48 mm, 24 mm, 12 mm, 6 mm, and 4 mm corresponding to the number of fins 24 (Fig. 8a), 60, 162 (Fig. 8b), 510 and 1050 (Fig. 8c) are

incorporated. The ratio of fin coverage area to total battery area is 0.008, 0.020, 0.053, 0.168 and 0.346, corresponding to the number fins 24, 60, 162, 510 and 1050, respectively.

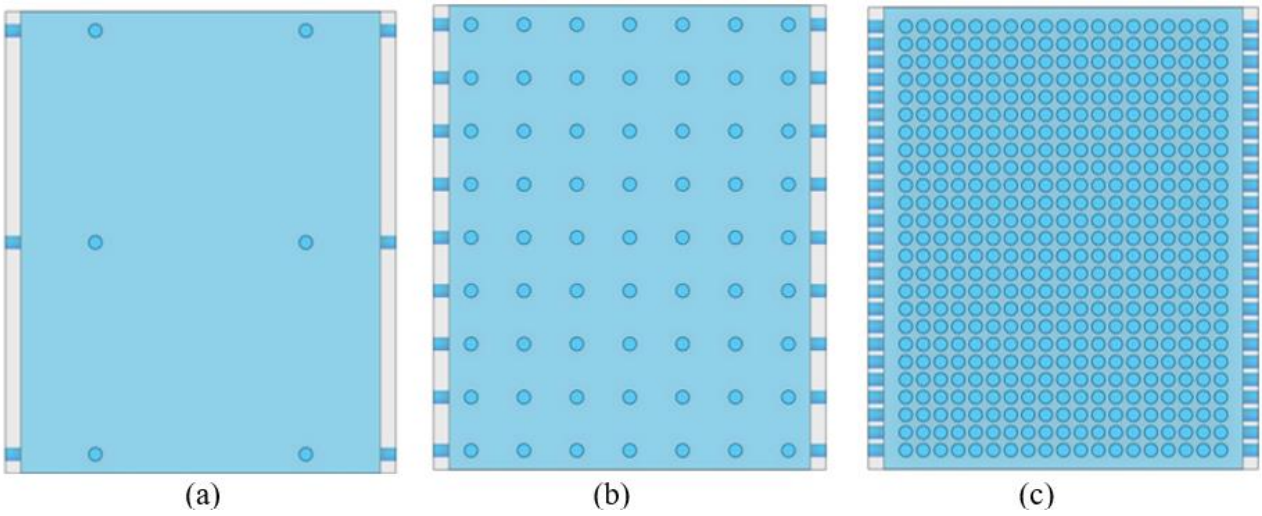

Fig. 8. PCM-Fin-Air BTMS with the different numbers of fins (a) 24 fins, (b) 162 fins, and (c) 1050 fins.

Fig. 9a shows that battery temperature is reduced with the number of fins. This is because with the number of fins increasing, the heat transfer in the PCM region is enhanced, increasing the PCM effective thermal conductivity [30], and then the interactions between fins and cooling air are increased, improving heat transfer from fins to air. The temperature is reduced sharply to 39.2 ℃ by increasing the fin number to 162, and that is associated with a slight increase in fan power to $0.0016\ W$, i.e., two times the fan power as compared to the 24 fins case. When the number of fins is 510 or even 1050, no significant decrease in battery temperature is noticed, but the fan power is dramatically increased to a much higher value of $0.017\ W$ (1050 fins case), nearly 21 times higher than 24 fins case.

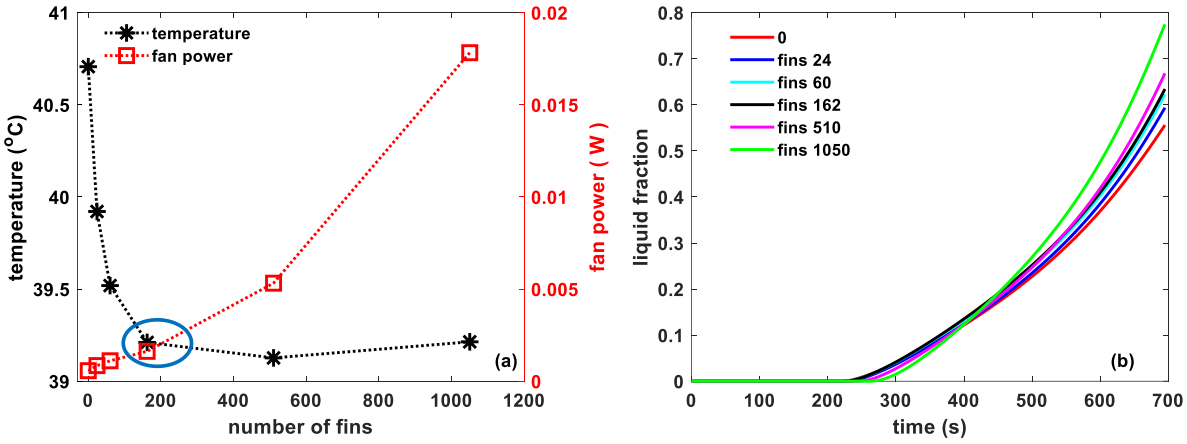

Fig. 9. Comparisons of (a) battery temperature and fan power (the ellipse represents the optimum value of number of fins) and (b) PCM liquid fraction for the different numbers of fins.

Furthermore, the PCM volume decreases as the number of fins increases, implying that the PCM cooling capacity would be reduced. In other words, the higher the fin number, the lower the effective latent of PCM. As shown in Fig. 9b, the PCM liquid fraction is highest for the 1050-fin case. Thus, having too many fins show the negative effect of decreased PCM volume and increased fan power. Hence, the results demonstrate that 162 fins case with pitch distance 12 mm can maintain nearly the lowest battery temperature while keeping the fan power consumption small (see marked ellipse in Fig. 9a) and is the best choice in all cases. Too many fins increase fan power multiple times and reduce PCM volume, which is not suitable for the long-term working of the battery.

4.3. Effects of fin diameter

To reveal the effects of fin diameter on the performance of PCM-Fin-Air BTMS, different values of fin diameter, including 0.5 mm (Fig. 10a), 1.0 mm, 3.0 mm (Fig. 10b) and 6.0 mm (Fig. 10c) corresponding to the ratio of fin coverage area to total battery area of 0.001, 0.006, 0.053 and 0.213, respectively, under the same constant number of fins 162 are used. The battery temperature and fan power for different values of diameter are shown in Fig. 11a, respectively. The temperature decreases with fin diameter, which is expected as the heat transfer area increases, dissipating more heat to airflow. However, too-thick fins may add excessive weight as the metal fins have a higher density than PCM and air, reducing PCM latent heat and increasing resistance to fluid flow.

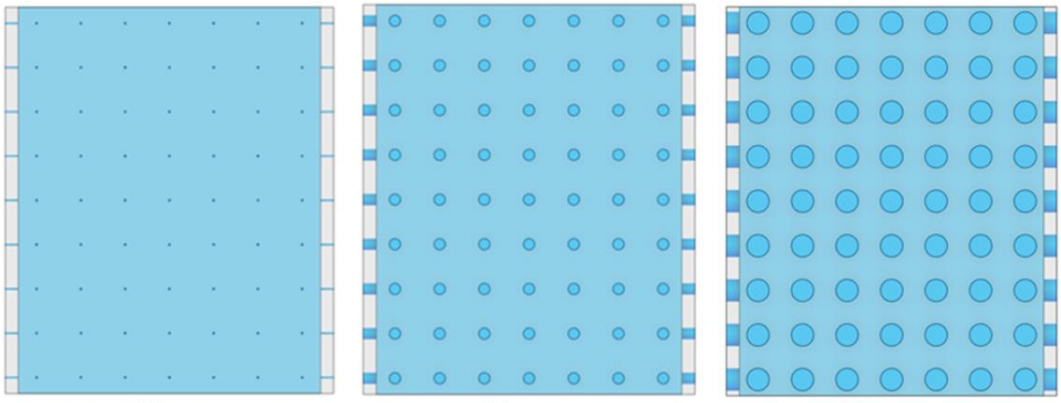

Fig. 10. PCM-Fin-Air BTMS with different values of fin diameter (a) 0.5 mm (b) 3.0 mm and (c) 6.0 mm.

It is clearly seen in Fig. 11a that the temperature is slashed by 0.74 ℃ when the fin diameter is increased from 0.5 mm to 3.0 mm at the small cost increase in fan power. When the fin diameter further changes to 6.0 mm, the temperature is not reduced significantly but the accompanying power consumption is sharply increased more than six times as compared to the 0.5 mm case. Furthermore, the PCM liquid fraction is highest for fin diameter 6.0 mm at the end of the discharge cycle, implying that in case of higher diameter,

the PCM will be quickest to run out. Thus, having a nearly lowest temperature at the cost of small fan power, the 3.0 mm fin diameter is found to be the optimum value (see ellipse in Fig. 11a).

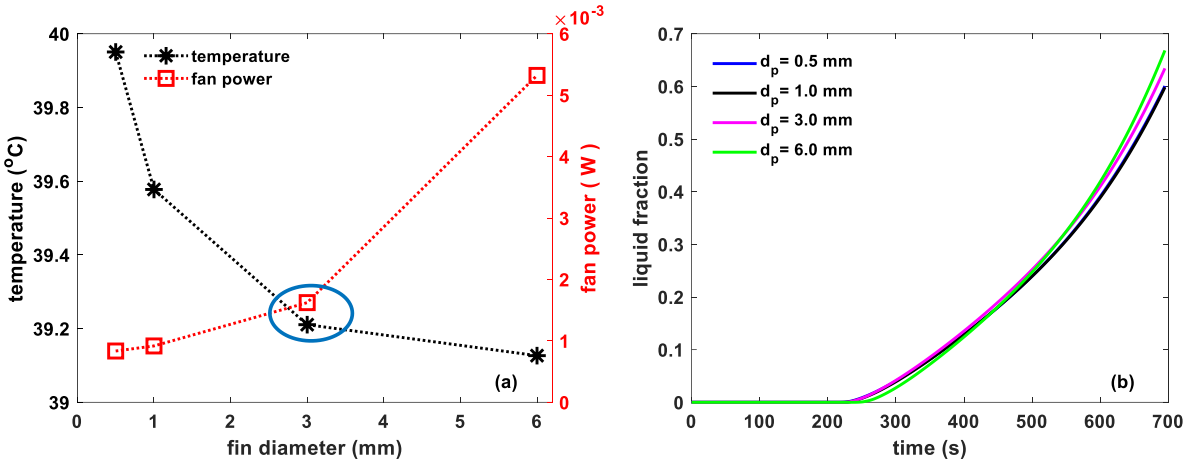

Fig. 11. Comparisons of (a) battery temperature and fan power (the ellipse represents the optimum value of fin diameter) and (b) PCM liquid fraction for different values of fin diameter.

4.4. Effects of inlet air velocity and temperature

The inlet velocity (u_{in}) and inlet temperature (T_{in}) are important controllable parameters that significantly affect the performance of BTMS [44, 47]. Four different values of velocity, including 0.1 m/s, 1.0 m/s, 2.0 m/s and 3.0 m/s and three different values of the temperature, i.e., 20 ℃, 25 ℃ and 30 ℃ are incorporated. The temperature value 30 ℃ is equal to ambient temperature, and to achieve an even lower temperature of inlet air corresponding to 25 ℃ and 20 ℃ air conditioning system could be used. When ambient air with an inlet temperature of 30 ℃ is directly used for cooling, the ideal fan power is calculated by Eq. (15). However, for the 25 ℃ and 20 ℃ cases, additional power consumed for lowering the air temperature must be taken into account. Then, the total power (Power consumption $P_c = P_{fan} + P_{ac}$) is sum of the ideal fan power (P_{fan}) and refrigerating power (P_{ac}).

To evaluate the refrigerating power, the refrigeration cycle of the air conditioning system is assumed to possess a constant coefficient of performance (COP) of 2 for all conditions [47, 48]. Therefore, the ideal refrigerating power is computed as follows [47]

$$P_{ac} = \dot{m}_{air} C_{p,air} \Delta T_{air} / COP \tag{16}$$

where $\dot{m}$ is the mass flow rate, ΔT is air, the temperature increase of the cooling air from the inlet to the outlet.

Fig. 12 shows the battery temperature at the end of the discharge cycle for different values of inlet temperature and velocity. At ambient inlet temperature and inlet velocity $0.1\ m/s$, the battery temperature is measured to be 39.4 ℃, and it is further dropped by 0.51 ℃ to value 38.9 ℃ if velocity is increased to $3.0\ m/s$. The decrease in temperature is attributed to enhanced air convection. The corresponding power consumption has raised up from $7.6 \times 10^{-6}\ W$ to $0.035\ W$.

As for the lower inlet temperature values 25 ℃ and 20 ℃ at low velocity $0.1\ m/s$, the battery temperature is observed to be 39.4 ℃ and 39.3 ℃, respectively. But the significant drop in battery temperature 1.08 ℃ and ~2 ℃ corresponding to inlet temperature values 25 ℃ and 20 ℃, respectively, are noted by increasing the velocity to $3.0\ m/s$. Which is accompanied by a sharp increase in total power (for example, power consumption is $0.035\ W$ at $0.1\ m/s$ and $6.7\ W$ at $3.0\ m/s$ for 25 ℃ case) as shown Fig. 12. This significant increase in power consumption is attributed to air conditioning that has to be turned on to produced cooled air.

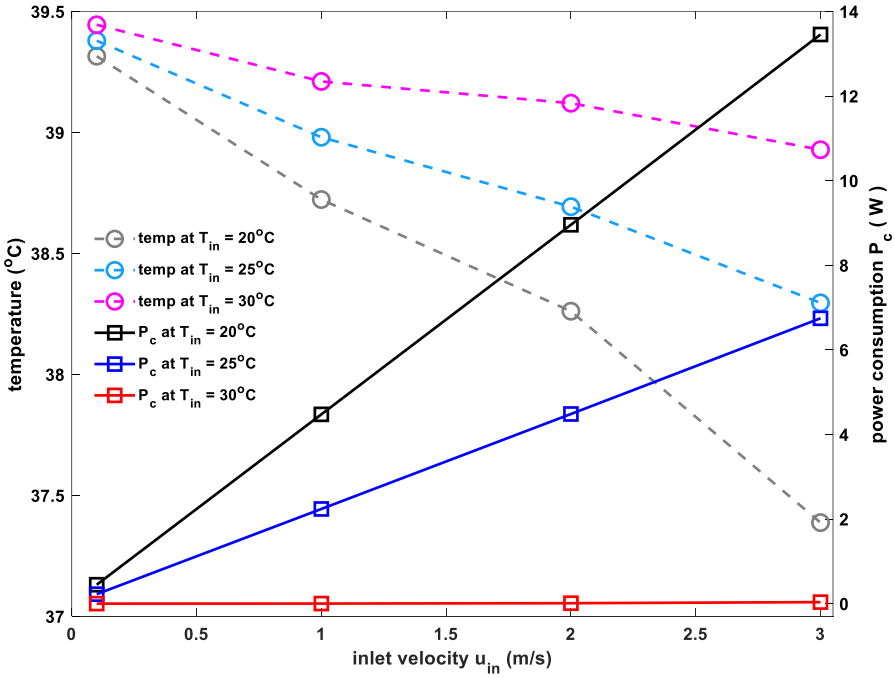

Fig. 12. Comparisons of battery temperature and power consumption at different inlet velocities and inlet temperature.

In addition, inlet air velocity and temperature also play significant roles in reducing the heat accumulation in PCM to prevent a complete melting scenario. The PCM liquid fraction for different values of velocity at inlet air temperatures of 30 ℃, 25 ℃ and 20 ℃ are shown in Fig. 13a-c. It is clearly observed in Fig. 13 that increasing velocity drops not only the battery temperature but also the PCM liquid fraction. The metal

pins are embedded in the PCM, and when the velocity of air flowing over the fins is increased, it takes away more heat which was previously accumulated in the PCM, resulting in the recovery of PCM latent heat. It is witnessed by the drop of PCM liquid fraction from 0.72 at air velocity 0.1 m/s by 21% when velocity is increased to 3.0 m/s.

Moreover, for the inlet temperatures of 25 ℃ and 20 ℃, the drop in PCM liquid fractions has become more pronounced. For temperature 20 ℃, the latent heat is recovered by 61% with a drop of liquid fraction from 0.67 to 0.06 when velocity is increased from 0.1 m/s to 3.0 m/s. Hence, it can be concluded that increasing the velocity and reducing inlet temperature greatly enhances the ability of the BTMS to control battery temperature and recover PCM latent heat, which is helpful for prolonging the safe working scenarios, improving battery life and reducing the risks of thermal runaway.

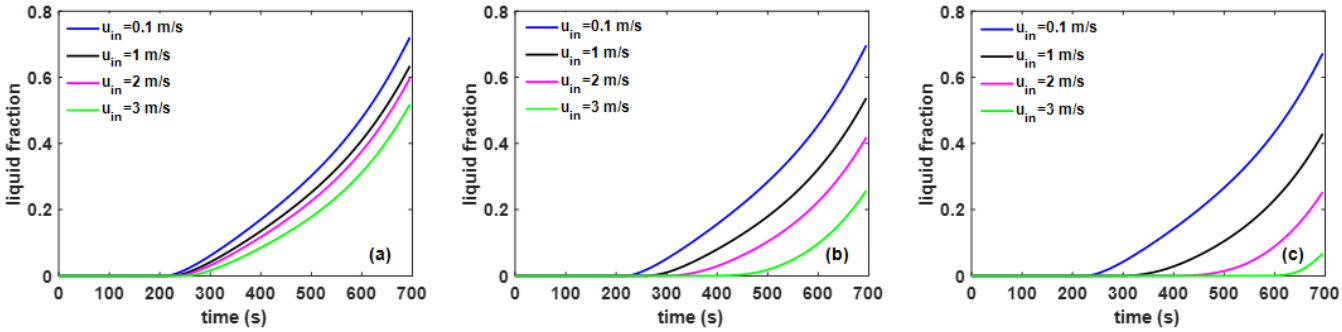

Fig. 13. Comparisons of PCM liquid fraction at different velocities for inlet temperature (a) $T_{in} = 30$ ℃ (b) $T_{in} = 25$ ℃ and (c) $T_{in} = 20$ ℃.

4.5. Cyclic thermal performance

It has been pointed out that the PCM heat dissipation capacity might be reliable for a single cycle, but it may deplete over time [49]. Therefore, cyclic tests are needed to be conducted to assess the thermal performance of novel hybrid PCM-Fin-Air BTMS under long-term workings conditions. In this work, one cycle consists of heating during battery discharge followed by the cooling time period [50]. The time for battery heating is 695 s, and that of cooling is two times of heating time, i.e., $t = 1390$ s. The cyclic testing is performed for three cycles at inlet temperature of 25 ℃ and two values of velocity, i.e., 1.0 m/s and 2.0 m/s, and the comparison of results for the novel PCM-Fin-Air BTMS, Fin-Air BTMS without PCM and PCM-Air BTMS without fins are presented in Fig. 14.

For the 1.0 m/s case, Fin-Air BTMS and PCM-Air BTMS completely fail to maintain battery temperature under 40 ℃ during all cycles. However, the PCM-Fin-Air has a maximum temperature (38.9 ℃) in the desired range and a maximum PCM liquid fraction of 0.64 during the first cycle. It can be seen in Fig. 14,

during the cooling time of the first cycle ($696 - 2085\ s$), the air cooling helps recover the PCM latent heat, and the liquid fraction drops to 0.25. But in the following two cycles, the PCM completely melts near the end of battery discharge time (see Fig. 14c), and the maximum temperature rises to 40.4 ℃ and 44.6 ℃ in the second and third cycles, respectively. However, it should be noted that the temperature of PCM-Fin-Air BTMS exceeded 40.0 ℃ for a much shorter time ($573\ s$) as compared to the PCM-Air BTMS ($1525\ s$) and Fin-Air BTMS ($2368\ s$) during three cycles.

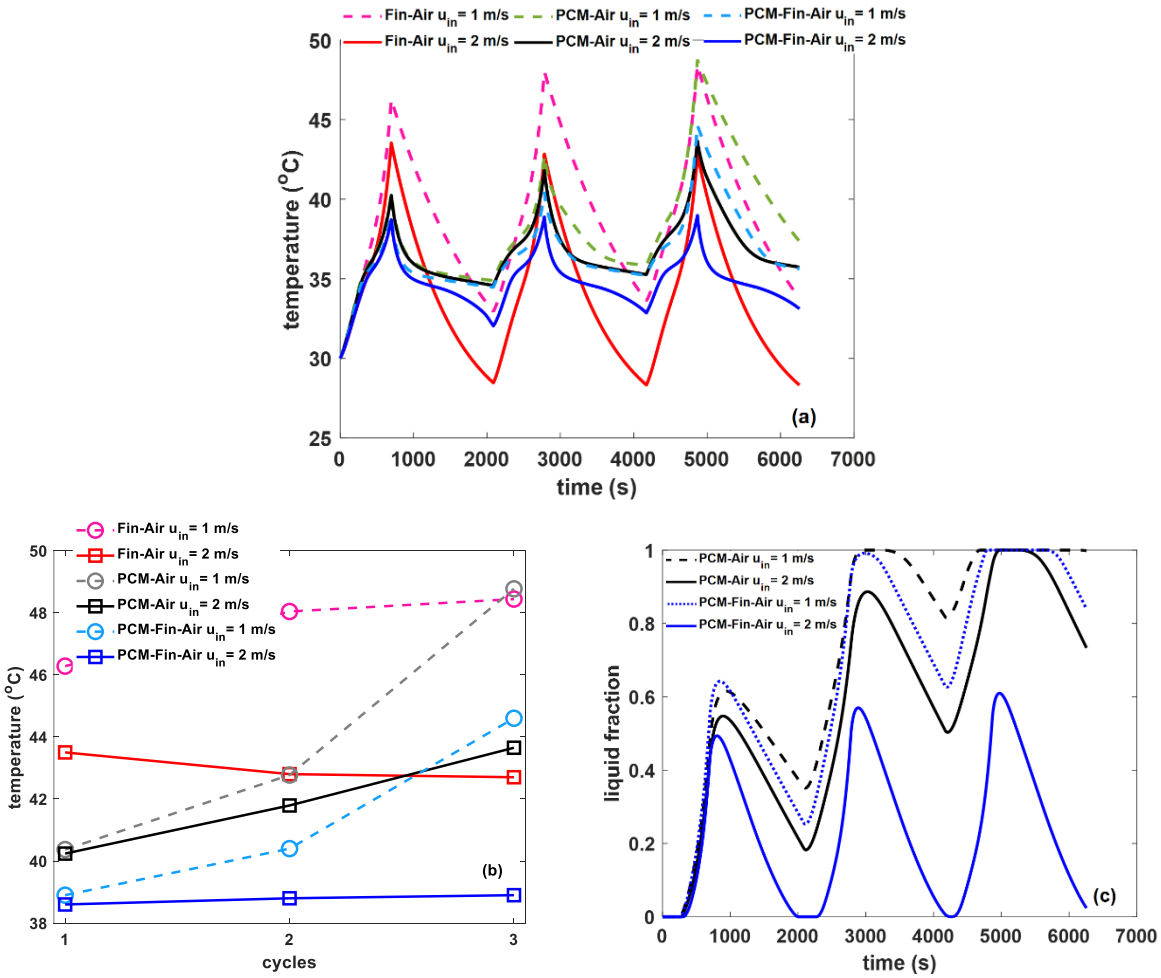

Fig. 14. Comparisons of (a) battery temperature (b) maximum battery temperature in each cycle and (c) PCM liquid fraction during cyclic tests at different inlet velocities.

As for the case of the velocity of $2.0\ m/s$, the maximum temperature values of 43.5 ℃, 42.8 ℃ and 42.7 ℃ are observed for Fin-Air BTMS in the first, second and third cycles, respectively. Next, the PCM-Air BTMS is also unable to reduce the maximum temperature below the desired value (see Fig. 14b). The PCM liquid fraction reaches unity in the third cycle, indicating that the lack of fins reduces the heat transfer to air. As a result, the complete melting of PCM is observed. Furthermore, the maximum temperature (43.65 ℃) in the third cycle for the PCM-Air BTMS becomes even higher than Fin-Air BTMS (42.7 ℃),

which is caused by comparatively less heat transfer from battery to air due to the lower thermal conductivity of pure PCM without fins.

On the other hand, PCM-Fin-Air BTMS has successfully restricted temperature under 40.0 ℃ during all cycles with maximum temperature values of 38.6 ℃, 38.8 ℃ and 38.9 ℃ in the first, second and third cycles, respectively. Moreover, in each cycle, PCM-Fin-Air BTMS is able to almost fully recover the PCM latent heat, which is witnessed by the nearly zero values of PCM liquid fraction near the time instants $2000\ s$ and $4250\ s$ and the maximum value of the PCM liquid fraction is observed to be 0.6 in the third cycle. PCM-Fin-Air BTMS is able to reduce the maximum temperature in the third cycle by 8.8% and 10.8% as compared to Fin-Air BTMS and PCM -Air BTMS, respectively. These results confirm that the novel hybrid PCM-Fin-Air BTMS has superior performance as compared to Fin-Air BTMS and PCM -Air BTMS.

5. Conclusions

In this work, a novel hybrid BTMS with PCM-embedded fins combined with forced air cooling over fins has been proposed. The performance of the novel hybrid BTMS is investigated through numerical simulations and compared to the BTMS without PCM and fins completely exposed to air cooling and BTMS with PCM and air cooling but no fins. The main conclusions drawn from this work are as follows:

1. The fins in the novel hybrid BTMS having higher thermal conductivity provide alternative pathways for heat flow. These new pathways improve heat dissipation by two methods: the heat transfer to deep layers of the PCM and air convection over the fin parts located in the air region, resulting in superior performance when compared to other BTMSs. The novel hybrid BTMS is shown to decrease battery temperature by 18.6% as compared to BTMS without PCM and fins completely exposed to air cooling and maintained the battery temperature under the desired value of 40 ℃.
2. It is observed that battery temperature is above 40 ℃ for thin PCMs but restricted to 39.2 ℃ at the optimum thickness $w_{PCM}\sim 1.0\ mm$ with less fan power, and the temperature does not increase appreciably with further increase in thickness.
3. Increasing fin diameter and fin number can decrease the battery temperature, which is due to improved thermal conductivity and larger heat transfer area enhancing the air convection cooling over fins. It is found that BTMS can maintain nearly the lowest battery temperature at suitable fin number 162 with a pitch distance of $12\ mm$ and diameter of $3\ mm$ with less fan power.
4. The cyclic tests are carried out, which show the superior performance of novel hybrid BTMS over the BTMS without PCM and fins completely exposed to air cooling. It has successfully maintained

the battery temperature and is able to nearly fully recover PCM latent heat in each cycle at moderate inlet velocity 2.0 m/s. It showed superior performance lowering the battery temperature by 8.8% and 10.8% as compared to Fin-Air BTMS and PCM -Air BTMS, respectively.

This study may provide new insights into the advanced design of BTMS for applications in battery energy storage systems for electric vehicles and renewable energy power stations.

Declaration of conflict of interests

The author(s) hereby declare no potential conflicts of interest with respect to the research, authorship and/or publication of this article.

Acknowledgments

The work described in this paper was supported by grants from the National Key R&D Program of China (2022YFE0207400), the Hong Kong Research Grants Council Early Career Scheme (25205519), and the Shenzhen Science and Technology Program (JCYJ20210324131006017).

References

[1] W. Li, Y. Xie, X. Hu, M.K. Tran, M. Fowler, S. Panchal, J. Zheng, K. Liu, An internal heating strategy for lithium-ion batteries without lithium plating based on self-adaptive alternating current pulse, IEEE Transactions on Vehicular Technology, (2022) 1-14.

[2] H. Liu, Z. Wei, W. He, J. Zhao, Thermal issues about Li-ion batteries and recent progress in battery thermal management systems: A review, Energy Conversion and Management, 150 (2017) 304-330.

[3] A.A. Pesaran, Battery thermal models for hybrid vehicle simulations, Journal of Power Sources, 110(2) (2002) 377-382.

[4] S. Du, Y. Lai, L. Ai, L. Ai, Y. Cheng, Y. Tang, M. Jia, An investigation of irreversible heat generation in lithium ion batteries based on a thermo-electrochemical coupling method, Applied Thermal Engineering, 121 (2017) 501-510.

[5] Y. Shi, S. Ahmad, H.Q. Liu, K.T. Lau, J.Y. Zhao, Optimization of air-cooling technology for LiFePO4 battery pack based on deep learning, Journal of Power Sources, 497 (2021).

[6] K. Chen, Y. Chen, Y. She, M. Song, S. Wang, L. Chen, Construction of effective symmetrical air-cooled system for battery thermal management, Applied Thermal Engineering, 166 (2020) 114679.

[7] Y. Xie, Y. Liu, M. Fowler, M.-K. Tran, S. Panchal, W. Li, Y. Zhang, Enhanced optimization algorithm for the structural design of an air-cooled battery pack considering battery lifespan and consistency, International Journal of Energy Research, 46(15) (2022) 24021-24044.

[8] S.A. Khan, C. Eze, K. Dong, A.R. Shahid, M.S. Patil, S. Ahmad, I. Hussain, J. Zhao, Design of a new optimized U-shaped lightweight liquid-cooled battery thermal management system for electric vehicles: A machine learning approach, International Communications in Heat and Mass Transfer, 136 (2022) 106209.

[9] S.A. Khan, S. Ahmad, K.T. Lau, K. Dong, S. He, H. Liu, J. Zhao, A novel strategy of thermal management system for battery energy storage system based on supercritical CO2, Energy Conversion and Management, 277 (2023) 116676.

[10] H.Q. Liu, S. Ahmad, Y. Shi, J.Y. Zhao, A parametric study of a hybrid battery thermal management system that couples PCM/copper foam composite with helical liquid channel cooling, Energy, 231 (2021).

[11] K.J. Kelly, M. Mihalic, M. Zolot, Battery usage and thermal performance of the Toyota Prius and Honda Insight during chassis dynamometer testing, in: Seventeenth Annual Battery Conference on Applications and Advances. Proceedings of Conference (Cat. No.02TH8576), 2002, pp. 247-252.

[12] J. Luo, D. Zou, Y. Wang, S. Wang, L. Huang, Battery thermal management systems (BTMs) based on phase change material (PCM): A comprehensive review, Chemical Engineering Journal, 430 (2022) 132741.

[13] S. Panchal, I. Dincer, M. Agelin-Chaab, R. Fraser, M. Fowler, Experimental and theoretical investigation of temperature distributions in a prismatic lithium-ion battery, International Journal of Thermal Sciences, 99 (2016) 204-212.

[14] V. Talele, M.S. Patil, S. Panchal, R. Fraser, M. Fowler, S.R. Gunti, Novel metallic separator coupled composite phase change material passive thermal design for large format prismatic battery pack, Journal of Energy Storage, 58 (2023) 106336.

[15] Z. Rao, Q. Wang, C. Huang, Investigation of the thermal performance of phase change material/mini-channel coupled battery thermal management system, Applied Energy, 164 (2016) 659-669.

[16] W. Zhang, Z. Liang, W. Wu, G. Ling, R. Ma, Design and optimization of a hybrid battery thermal management system for electric vehicle based on surrogate model, International Journal of Heat and Mass Transfer, 174 (2021) 121318.

[17] S. Al Hallaj, J.R. Selman, Thermal management of battery systems, US Patent 6468689 B1, (2002).

[18] Y. Zhang, J. Wang, X. Yang, H.M. Ali, Z. Said, C. Liu, Fabrication of shape-stabilized phase change materials based on waste plastics for energy storage, Journal of Energy Storage, 52 (2022) 104973.

[19] H.M. Ali, Phase change materials based thermal energy storage for solar energy systems, Journal of Building Engineering, 56 (2022) 104731.

[20] M.A. Bamdezh, G.R. Molaeimanesh, Impact of system structure on the performance of a hybrid thermal management system for a Li-ion battery module, Journal of Power Sources, 457 (2020) 227993.

[21] Z. Ling, F. Wang, X. Fang, X. Gao, Z. Zhang, A hybrid thermal management system for lithium ion batteries combining phase change materials with forced-air cooling, Applied Energy, 148 (2015) 403-409.

[22] H. Fathabadi, High thermal performance lithium-ion battery pack including hybrid active–passive thermal management system for using in hybrid/electric vehicles, Energy, 70 (2014) 529-538.

[23] M. Mehrabi-Kermani, E. Houshfar, M. Ashjaee, A novel hybrid thermal management for Li-ion batteries using phase change materials embedded in copper foams combined with forced-air convection, International Journal of Thermal Sciences, 141 (2019) 47-61.

[24] R.D. Jilte, R. Kumar, M.H. Ahmadi, L. Chen, Battery thermal management system employing phase change material with cell-to-cell air cooling, Applied Thermal Engineering, 161 (2019) 114199.

[25] Y. Lv, G. Liu, G. Zhang, X. Yang, A novel thermal management structure using serpentine phase change material coupled with forced air convection for cylindrical battery modules, Journal of Power Sources, 468 (2020) 228398.

[26] G. Jiang, J. Huang, M. Liu, M. Cao, Experiment and simulation of thermal management for a tube-shell Li-ion battery pack with composite phase change material, Applied Thermal Engineering, 120 (2017) 1-9.

[27] P. Qin, M. Liao, D. Zhang, Y. Liu, J. Sun, Q. Wang, Experimental and numerical study on a novel hybrid battery thermal management system integrated forced-air convection and phase change material, Energy Conversion and Management, 195 (2019) 1371-1381.

[28] R.A. Lawag, H.M. Ali, Phase change materials for thermal management and energy storage: A review, Journal of Energy Storage, 55 (2022) 105602.

[29] H.M. Ali, An experimental study for thermal management using hybrid heat sinks based on organic phase change material, copper foam and heat pipe, Journal of Energy Storage, 53 (2022) 105185.

[30] V.G. Choudhari, A.S. Dhoble, S. Panchal, Numerical analysis of different fin structures in phase change material module for battery thermal management system and its optimization, International Journal of Heat and Mass Transfer, 163 (2020) 120434.

[31] H.M. Ali, A. Arshad, Experimental investigation of n-eicosane based circular pin-fin heat sinks for passive cooling of electronic devices, International Journal of Heat and Mass Transfer, 112 (2017) 649-661.

[32] N. Khaboshan, F. Jaliliantabar, A.A. Abdullah, S. Panchal, Improving the Cooling Performance of Cylindrical Lithium-Ion Battery Using Three Passive Methods in a Battery Thermal Management System Available at SSRN 4276692, 2022.

[33] M.Y. Yazici, M. Avci, O. Aydin, Combined effects of inclination angle and fin number on thermal performance of a PCM-based heat sink, Applied Thermal Engineering, 159 (2019) 113956.

[34] R. Kalbasi, M. Afrand, J. Alsarraf, M.-D. Tran, Studies on optimum fins number in PCM-based heat sinks, Energy, 171 (2019) 1088-1099.

[35] Z. Sun, R. Fan, F. Yan, T. Zhou, N. Zheng, Thermal management of the lithium-ion battery by the composite PCM-Fin structures, International Journal of Heat and Mass Transfer, 145 (2019) 118739.

[36] F. Liu, J. Wang, Y. Liu, F. Wang, N. Yang, X. Liu, H. Liu, W. Li, H. Liu, B. Huang, Performance analysis of phase change material in battery thermal management with biomimetic honeycomb fin, Applied Thermal Engineering, 196 (2021) 117296.

[37] P. Ping, R. Peng, D. Kong, G. Chen, J. Wen, Investigation on thermal management performance of PCM-fin structure for Li-ion battery module in high-temperature environment, Energy Conversion and Management, 176 (2018) 131-146.

[38] J. Weng, Y. He, D. Ouyang, X. Yang, G. Zhang, J. Wang, Thermal performance of PCM and branch-structured fins for cylindrical power battery in a high-temperature environment, Energy Conversion and Management, 200 (2019) 112106.

[39] L. Sheng, H. Zhang, H. Zhang, L. Su, Z. Zhang, Lightweight liquid cooling based thermal management to a prismatic hard-cased lithium-ion battery, International Journal of Heat and Mass Transfer, 170 (2021) 120998.

[40] N. Javani, I. Dincer, G.F. Naterer, B.S. Yilbas, Heat transfer and thermal management with PCMs in a Li-ion battery cell for electric vehicles, International Journal of Heat and Mass Transfer, 72 (2014) 690-703.

[41] Z. Sun, R. Fan, N. Zheng, Thermal management of a simulated battery with the compound use of phase change material and fins: Experimental and numerical investigations, International Journal of Thermal Sciences, 165 (2021) 106945.

[42] Rubitherm Technologies Gmbh, Berlin, Germany, https://www.rubitherm.eu/en/index.php/productcategory/organische-pcm-rt.

[43] D. Kong, R. Peng, P. Ping, J. Du, G. Chen, J. Wen, A novel battery thermal management system coupling with PCM and optimized controllable liquid cooling for different ambient temperatures, Energy Conversion and Management, 204 (2020) 112280.

[44] P. Ping, Y. Zhang, D. Kong, J. Du, Investigation on battery thermal management system combining phase changed material and liquid cooling considering non-uniform heat generation of battery, Journal of Energy Storage, 36 (2021) 102448.

[45] N.O. Moraga, J.P. Xamán, R.H. Araya, Cooling Li-ion batteries of racing solar car by using multiple phase change materials, Applied Thermal Engineering, 108 (2016) 1041-1054.

[46] W.L.-F.W.L.-Y. Yuan Hao, Battery Thermal Management System with Liquid Cooling and Heating in Electric Vehicles, Journal of Automotive Safety and Energy, 3(4) (2012) 371-380.

[47] F. Chen, R. Huang, C. Wang, X. Yu, H. Liu, Q. Wu, K. Qian, R. Bhagat, Air and PCM cooling for battery thermal management considering battery cycle life, Applied Thermal Engineering, 173 (2020) 115154.

[48] M. Shams-Zahraei, A.Z. Kouzani, S. Kutter, B. Bäker, Integrated thermal and energy management of plug-in hybrid electric vehicles, Journal of Power Sources, 216 (2012) 237-248.

[49] J. Liu, Y. Fan, Q. Xie, An experimental study on the thermal performance of mixed phase change materials-based battery cooling system, Journal of Energy Storage, 46 (2022) 103839.

[50] R. Fan, N. Zheng, Z. Sun, Evaluation of fin intensified phase change material systems for thermal management of Li-ion battery modules, International Journal of Heat and Mass Transfer, 166 (2021) 120753.